Research Article

Nano Biomed Eng

Preparation and Investigation of Structural and Optical Properties of Poly(methyl methacrylate)/ Indium Oxide Nanocomposites for Antibacterial Application

Musaab Khudhur Mohammed[1], Noor Ali Sami[1], Mohanad Abdul Salam[2], Reem Tuama Yousif[3], Khansaa Haleem Mohsin[1]

[1] Department of Physics, College of Education for Pure Sciences, University of Babylon, Babylon, Iraq
[2] Ministry of Education, Directorate General of Education Rusafa, Iraq
[3] Department of Physics, College of Sciences, University of Babylon, Babylon, Iraq

Corresponding author. E-mail: pure.musaab.kh@uobabylon.edu.iq

Received: Jan. 4, 2024; **Revised:** Feb. 14, 2024; **Accepted:** Mar. 6, 2024

Citation: M.K. Mohammed, N.A. Sami, M.A. Salam, et al. Preparation and investigation of structural and optical properties of poly(methyl methacrylate)/ indium oxide nanocomposites for antibacterial application. *Nano Biomedicine and Engineering*, 2024.

http://doi.org/10.26599/NBE.2024.9290079

Abstract

This study describes the preparation of poly(methyl methacrylate) (PMMA) composites reinforced with various loadings (0 wt.%, 1.2 wt.%, 2.4 wt.%, and 3.6 wt.%) of indium oxide (In_2O_3) using solution casting. Fourier-transformation infrared spectroscopy was used to analyze the structural characteristics of the nanocomposite and confirm the physical interactions between In_2O_3 nanoparticles (NPs) and the PMMA matrix. Field emission scanning electron microscopy was used to examine the nanocomposite surface and showed that the In_2O_3 NPs were distributed and homogenous through the PMMA matrix. An increase in the ratio of In_2O_3 NPs in the PMMA changed the optical characteristics with an increase in the absorbance, absorption coefficient, refractive index, extinction coefficient, and real and imaginary dielectric constants and a decrease in the transmittance and indirect energy gap. The absorption coefficient was $< 10^4$ cm^{-1}, confirming the indirect electron transition. The antibacterial effect of PMMA/In_2O_3 films were examined against Gram-positive *Staphylococcus aureus* and Gram-negative *Escherichia coli* and demonstrated an increase in inhibition zone diameter with an increase in In_2O_3 NP content. Thus, the PMMA/In_2O_3 nanocomposite exhibited antibacterial activity.

Keywords: poly (methyl methacrylate) (PMMA); In_2O_3 nanoparticles; optical characteristics; *Escherichia coli*; *Staphylococcus aureus*

Introduction

Polymer nanocomposites are polymers that have been enhanced through the incorporation of fillers with diverse geometries (e.g., platelets, fibers, or spheroids) that are < 100 nm in at least one dimension [1]. Nanocomposites, resulting from the combination of various materials, structures, and compositions, display a broad spectrum of properties that are highly suitable for multiple applications. Consequently, considerable interest has increased in multifunctional materials within the nanocomposite sector [2].

Poly(methacrylates) are polymers derived from the

esters of methacrylic acid and have the chemical formula $(C_5H_8O_2)_n$ [1], of which poly(methyl methacrylate) (PMMA), is the most used. PMMA is a standard polymer with a long history of usage [2,3]. PMMA is neutral and translucent at 1.15–1.19 g/cm^3 [4]. PMMA is used as a structural resource in orthopedics and orthodontia; other polymers that can be used for this purpose include polyethylene and poly-ether-ether-ketone, and polymethacrylate often exhibits poorer motorized strength when compared with these two former options. The superior adaptability of PMMA in many studies compensates for its disadvantage [5]. PMMA has emerged as the most useful polymer for disposable contact lenses because of the cost-effectiveness, chemical and photochemical toughness, and exceptional light transmission within the visible range [6]. PMMA has received endorsement for usage in biomedical applications because of the nontoxic nature, long-lasting chemical stability, and favorable mechanical qualities. PMMA is usually physiologically inert and often does not elicit inflammatory responses in tissues [7].

Metal oxide nanoparticles (NPs) possess unique properties and are employed in medical research and scientific studies because of their intriguing qualities and superior benefits in comparison with larger-sized materials [8]. Recent research suggests that incorporating nanooxide into organic polymers can enhance their physical and optical properties while also providing resistance against cracking and aging caused by environmental stress. The antibacterial properties of thin films of indium oxide (In_2O_3) are evident in their ability to disrupt the organization of bacterial cell membranes and regulate the activity of membrane-bound enzymes. Consequently, they have been used to eliminate the Gram-negative bacterium *Escherichia coli*, suggesting potential applications in the treatment of infectious diseases [9]. In_2O_3 is a semiconductor that exhibits n-type conductivity and has a wide band gap. Semiconductors have garnered considerable interest because of their controversial inherent material properties, including their broad energy band gap from 3.4 to 3.7 eV [10]. In stoichiometric circumstances, In_2O_3 frequently exhibits insulating properties. Nevertheless, in the nonstoichiometric form, In_2O_3 transitions to a semiconductor state characterized by substantial conductivity [11]. In_2O_3 is recognized as a transparent conductor that has attracted considerable attention because of the low effective mass of its electron. The key characteristics of these features have produced an increasing range of applications in the manufacturing of solar cells, antimicrobial treatments [12], and sensors [13].

The antibacterial activity of a material or chemical relates to the capacity to eradicate or impede the proliferation of bacteria. Most antibacterial drugs available in the current market are either artificially produced or derived from living organisms [14]. However, hybrid nanocomposites have also been assessed for their antibacterial efficacy against a diverse range of bacterial and fungal species. To exert their antimicrobial effects, NPs must have an intimate contact with bacterial cells via interactions such as electrostatic attractions, van der Waals forces, receptor-ligand interactions, and hydrophobic interactions [15]. NPs infiltrate the bacterial membrane and interact with key metabolic pathways to induce alterations to the structure and functionality of the cell membrane. Within the bacterial cell, the NPs engage with DNA, lysosomes, ribosomes, and enzymes. This interaction induces oxidative stress, abnormalities in cell membrane permeability, disturbances in electrolyte balance, inhibition of enzymes, deactivation of proteins, and inconsistencies in gene expression [16].

Many researchers have reported syntheses of nanocomposites for antibacterial applications. Mohammed et al. prepared a PMMA/Si_3N_4/TaC nanocomposite by using the casting method, investigated the structural and optical properties, and examined the antibacterial application. They found that the inhibition zone for *Staphylococcus aureus* and *Klebsiella aerogenes* increased with increasing concentrations of Si_3N_4/TaC NPs [17].

Kadim et al. studied the effect of corn starch NPs on the morphological, optical, and dielectric behaviors of a PVA/PMMA/PAAM polymer blend by using the casting method for optoelectronic and antibacterial applications. The incorporation content of CSNPs into the polymer blend enhanced the bioactivity of the composite. The sizes of the inhibitory zones caused by *S. aureus* were 0, 26, and 32 mm for solutions containing 0 wt.%, 2 wt.%, and 4 wt.% CSNPs, respectively [18].

In this study, we prepared a PMMA/In_2O_3

nanocomposite, investigated the structural and optical properties, and applied it in antibacterial applications.

Experimental

Materials

Pure PMMA (Alpha Chemika, India) with an average molecular weight of 120 000 g/mol was used in a granular form. In_2O_3 NPs (Sigma Aldrich) (99.8% pure) formed a white powder 40-nm particle size and was insoluble in water.

Preparation of nanocomposites

PMMA (1 g) was dissolved in chloroform (50 mL) for 30 min at room temperature (RT) and incubated for another 10 min at 75–80 °C with stirring. The resulting solution was cast onto clean glass Petri dishes and maintained under air at RT for 240 h until the solvent was completely evaporated. PMMA/In_2O_3 NPs were also prepared via the same procedure to produce nanocomposite films. The method is summarized in Table 1. The average thickness of the produced films was approximately 0.10 mm.

Table 1 Preparation of pure PMMA and nanocomposite films

In_2O_3 (wt.%)	PMMA (g)	In_2O_3 (g)
0	1	0
1.2	0.988	0.012
2.4	0.976	0.024
3.6	0.964	0.036

Characterization

Fourier-transformation infrared (FTIR) spectroscopy was used to examine the chemical composition of the prepared samples (Bruker business, type vertex-70 spectrometer, Germany) at RT in the range of 500–4 000 cm^{-1}. Field emission scanning electron microscopy (FE-SEM; INSPECT S50, firm, Japan origin, type FEI Customer ownership) was used to determine the surface morphology of the films. A Shimadzu UV-1650 PC spectrophotometer (Phillips, Japan) was used to examine the development of nanocomposite at wavelengths ranging from 200 to 1 100 nm. The antibacterial efficacy of the nanocomposite films was evaluated against two clinical pathogens, *E. coli* and *S. aureus*.

Result and Discussion

Figure 1 illustrates rhe optical absorbance of pure PMMA and PMMA/In_2O_3 nanocomposites as a film were measured at 200–1 100 nm. All samples display markedly greater absorption in the ultraviolet region than that of PMMA. At elevated energy levels (eV) (specifically, at 200 nm), the donor material stimulated the movement of electrons into the conduction band. This phenomenon took place when the electrons assimilated a photon of a certain energy, causing their shift from a lower energy state to a higher one. Additionally, the absorbance was enhanced by increasing the contribution ratio from 0 wt.% to 3.6 wt.% In_2O_3 NPs. At high energies (eV), the absorbance increased from 0.66 to 0.92 (39.39%) at increasing concentrations of 0 wt.% to 3.6 wt.% for In_2O_3 NPs, whereas at low energies (340–1 100 nm), the absorbance decreased to 0.0.6 and 0.30 for 0 wt.% and 3.6 wt.% In_2O_3 NPs, respectively. This may be attributed to the insufficient energy of incident photons at longer wavelengths that prevent them from interacting with atoms and thereby allows the photon to be transmitted. These results are consistent with those in the literature [19, 20].

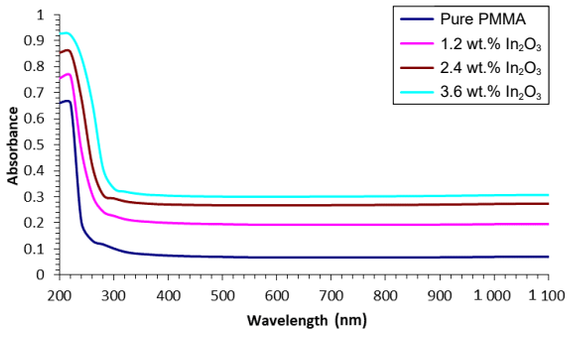

Fig. 1 Absorbance of pure PMMA and PMMA/In_2O_3 nanocomposite with wavelength.

The transmittance (T) is given by the following equation [21]:

$$T = e^{-\alpha t} \quad (1)$$

where α is the absorption coefficient and t is the thickness of film. The transmittance spectra of PMMA/In_2O_3 nanocomposites at various wavelengths are shown in Fig. 2 and demonstrate a notable increase in transmittance as the wavelength increases, namely in the vicinity of 340 nm. After this point, the transmission experiences a relatively stable and consistent increase. Data unequivocally indicates that the inclusion of In_2O_3 reduced the transmittance of

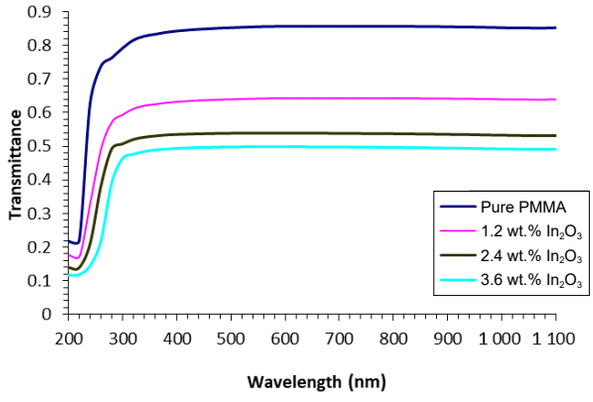

Fig. 2 Transmittance of pure PMMA and PMMA/In_2O_3 nanocomposite.

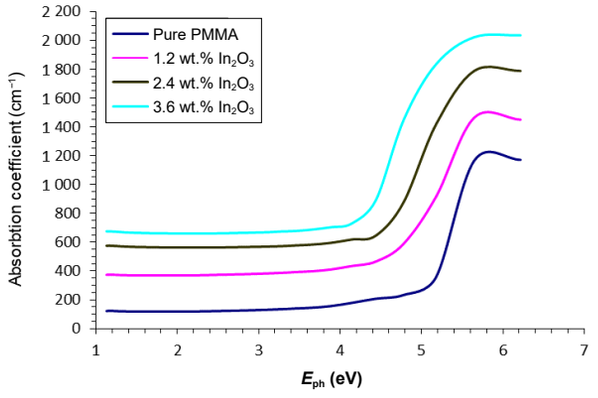

Fig. 3 Absorption coefficient of pure PMMA and PMMA/In_2O_3 nanocomposite with photon energy.

light. Increasing the proportion of In_2O_3 in the PMMA matrix improved the observed behavior, explaining the rise in light absorption and decline in transmittance caused by the enhancement with nanomaterials, which agrees with the previous studies [22].

The absorption coefficient of the polymer PMMA and nanocomposite films is used as a diagnostic instrument to measure the reduction in light intensity within the film. Alternatively, α is a sensitive physical approach that provides valuable information on the type of charges present in a band and the amount of the band gap energy. This information depends on the energy of the input light. The absorption coefficient was calculated using an empirical correlation [22]:

$$\alpha = 2.303\frac{A}{t} \tag{2}$$

where A is the absorbance. The relationship between the absorption coefficient of PMMA/In_2O_3 nanocomposite films and photon energy is shown in Fig. 3. The absorption coefficient exhibited a steady rise in value with increasing photon energy, eventually reaching 4.14 eV. The lower transition of electrons occurs when the energy of the incident photon is insufficient for moving the electron from the valence band to the conduction band. Upon attaining an energy level of 4.14 eV, the absorption coefficient of all samples demonstrates a notable augmentation. The electron undergoes significant transitions inside the conductive band, which can be attributed to this phenomenon. The absorption value was $< 10^4$ cm^{-1}, indicating the indirect transition occurred.

The index of refractive (n) was calculated as follows [23]:

$$n = \frac{1+\sqrt{R}}{1-\sqrt{R}} \tag{3}$$

where R is the reflectance. The refractive index of PMMA/In_2O_3 nanocomposites vs. wavelength is shown in Fig. 4. Incorporating In_2O_3 into the polymer matrix increased the refractive index of the samples, and aberrant dispersion in the spectral region < 280 nm and normal dispersion in the spectral range > 280 nm were possible. The resonance phenomenon occurring between the polarization of the incoming light and the electrons in PMMA/In_2O_3 is an atypical behavior, and subsequently electrons are linked to the oscillating electromagnetic field. The values of the refractive index also increased as the amount of In_2O_3 NPs increased. This behavior agrees with that seen in the previous studies [24].

The energy gap is given by [25]

$$(\alpha h\upsilon)^{1/m} = C(h\upsilon - E_g) \tag{4}$$

where C is constant, the photon energy is denoted as $h\upsilon$, the energy gap is represented as E_g, and m can take values of 2 and 3 for allowed and forbidden indirect transitions, respectively.

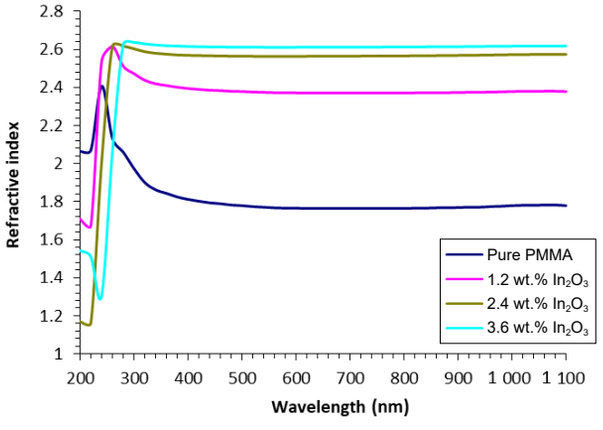

Fig. 4 Refractive index of pure PMMA and PMMA/In_2O_3 nanocomposite.

The determination of the band gap energy (E_g) involves plotting a graph that relates the product of the absorption coefficient (αhv) and the photon energy (hv). The value of m in this equation can be either (1/2) or (1/3) depending on whether the electron transition is allowed or forbidden, respectively. The optical band gap values are determined by extrapolating the linear segments of these relationships to the hv axis and are documented in Table 2. Figs. 5 and 6 illustrate the indirect band gap of both the pure PMMA and PMMA/In_2O_3 nanocomposite. These figures demonstrate that the E_g values decreased with the rise in the concentration of In_2O_3 NPs. The allowed indirect energy gap decreased from 4.7 to 3.28 eV while the forbidden indirect energy gap decreased from 4.6 to 3.18 eV. The possibility of localized states of different color centers extending into the mobility gap explains this outcome. This result agrees with those in previous studies [26,27].

The extinction coefficient (k) is given by the equation [28]:

$$k = \alpha\lambda/4\pi \quad (5)$$

where λ is the wavelength. Fig. 7 shows the extinction coefficient as a function of the wavelength for all prepared films. The extinction coefficient for PMMA/In_2O_3 nanocomposites has a prominent peak at lower energies, specifically at 240 nm and then decreases at 320 nm. Above 320 nm, the extinction coefficient increased linearly with increasing content of In_2O_3 NPs. The concurrent rise in photon energy may explain this behavior. The correlation between the concentration ratio of In_2O_3 NPs and the extinction coefficient of nanocomposites is readily apparent. An increase in the absorption of incoming light explains this phenomenon [29].

The dielectric constant is composed of two parts: the real part (ε_1) and the imaginary part (ε_2) [30]:

$$\varepsilon_1 = n^2 - k^2 \quad (6)$$

$$\varepsilon_2 = 2nk \quad (7)$$

Figs. 8 and 9 depict the fluctuations found in the real (ε_1) and imaginary components (ε_2) of the dielectric constant for the PMMA/In_2O_3 nanocomposites. The data indicates that the dielectric constant of pure PMMA polymer has greater values for both the real and imaginary components at shorter wavelengths that diminish as the wavelength

Table 2 E_g^{opt} Values for the allowed and forbidden energy gap at the optimum value of pure PMMA and PMMA/In_2O_3 nanocomposites

In_2O_3 (wt.%)	Allowed E_g (eV)	Forbidden E_g (eV)
0	4.7	4.6
1.2	3.88	3.61
2.4	3.63	3.4
3.6	3.28	3.18

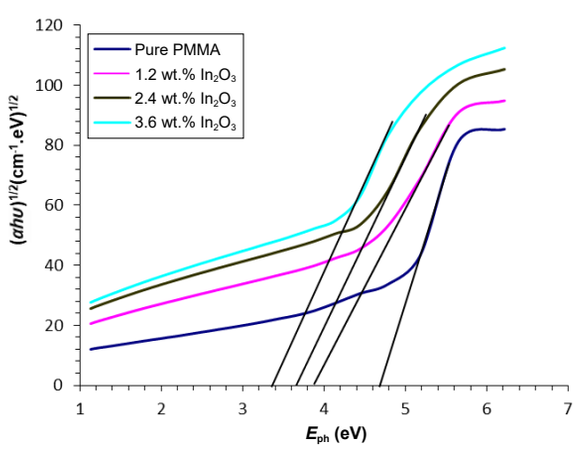

Fig. 5 Relationship between $(\alpha hv)^{½}$ vs. (hv) for pure PMMA and PMMA/In_2O_3 nanocomposites.

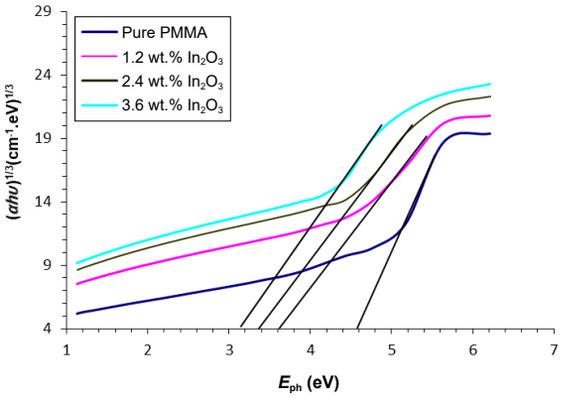

Fig. 6 Relationship between $(\alpha hv)^{1/3}$ versus (hv) for pure PMMA and PMMA/In_2O_3 nanocomposites.

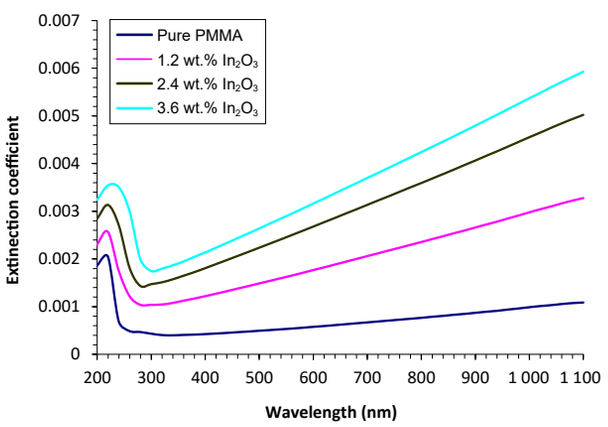

Fig. 7 Extinction coefficient of PMMA/In_2O_3 nanocomposites.

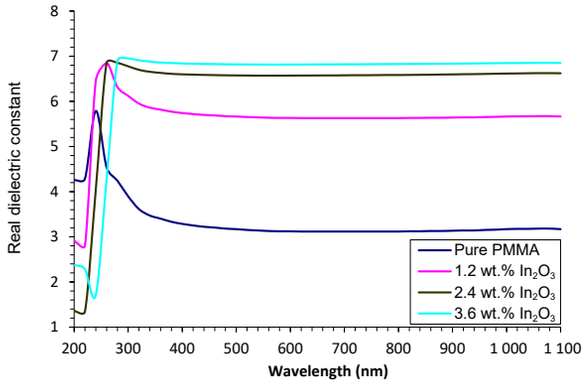

Fig. 8 Real dielectric constant of PMMA/In_2O_3 nanocomposites.

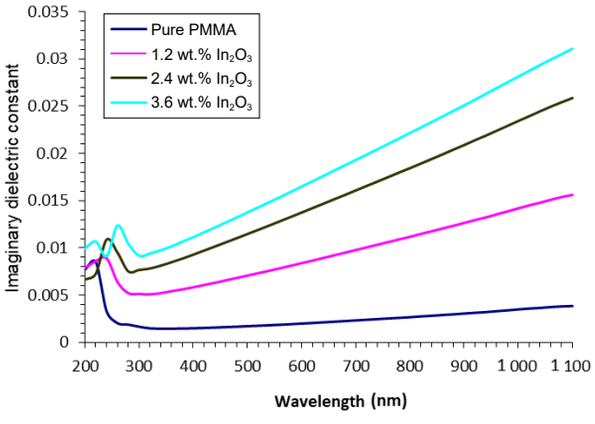

Fig. 9 Imaginary dielectric constant of PMMA/In_2O_3 nanocomposites.

increased. The nanocomposite films displayed a prominent increase in both the real and imaginary values as the wavelength decreased. This is followed by a substantial decrease in higher energy levels. The magnitudes of n predominantly influence the effective dielectric constant, considering that the latter values (k) are considerably less than the refractive index, particularly when squared [31].

The optical conductivity (σ_{op}) is defined by [32]

$$\sigma_{op} = \alpha nc/4\pi \quad (8)$$

where c is the speed of light. Fig. 10 depicts the optical conductivity of the PMMA/In_2O_3 nanocomposites. The pure PMMA polymer demonstrates a notable enhancement in optical conductivity at shorter wavelengths, followed by a reduction at longer wavelengths, which is explained by the concurrent increase in the absorption coefficient. The observed optical conductivity is directly proportional to the concentration of In_2O_3 NPs. The observed phenomena can be attributed to the rise in the absorption coefficient [33, 34].

The composition of the newly prepared pure

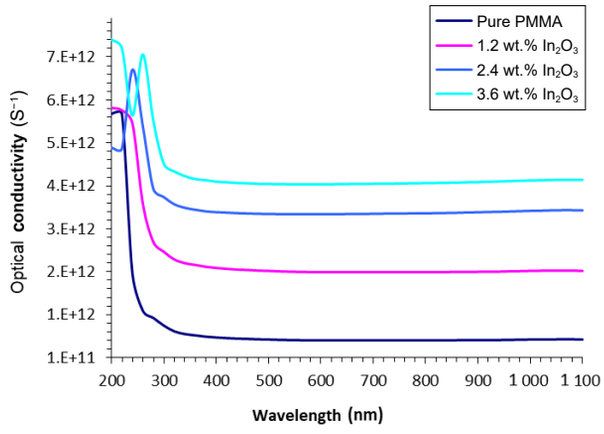

Fig. 10 Optical conductivity of PMMA/In_2O_3 nanocomposites.

PMMA and PMMA/In_2O_3 nanocomposite was verified via FTIR spectroscopy. The FTIR spectra of pure PMMA and PMMA with various content of In_2O_3 NPs from 500–4 000 cm^{-1} are shown in Figs. 11(a)–11(d). The absorption band of pure PMMA in Fig. 11(a) at 3 032 cm^{-1} corresponds to the CH_3 asymmetric stretching vibrations. The band at 1 685.48 cm^{-1} was attributed to the C=C stretching vibration while the bands 1 214.48 and 1 148 cm^{-1} corresponded to the C–C–O and C–O–C asymmetric stretches, respectively. The bands at 744.03 and 687.52 cm^{-1} were assigned to the C=C stretch and the deformation vibrations (CCO) in the plane (bending) [35–37]. The increasing concentration of 1.2 wt.%, 2.4 wt.%, and 3.6 wt.% In_2O_3 NPs to PMMA polymer (Figs. 11(b)–11(d)) caused a change in intensities in several bands and shifts in other bands and thus caused a physical interaction with the polymer matrix. The FTIR spectra demonstrated that no chemical interactions occurred between the PMMA polymer matrix and In_2O_3 NPs. This result is consistent with that in a previous study [38].

FE-SEM was used to examine the distribution of NPs within the polymer and then verify the effect of these In_2O_3 NPs on the nanocomposites. Fig. 12 shows FE-SEM images of films made from PMMA/In_2O_3 nanocomposites with varying amounts of In_2O_3 NPs. Fig. 12(a) shows that the surface polymer was smooth and homogenous, indicating that the fabrication was successful while in Figs. 12(b)–12(d), the In_2O_3 NPs are shown distributed throughout the polymer matrix, and this distribution increases with the increasing concentration of In_2O_3 NPs. The results establish the surface morphology of the membranes (PMMA/In_2O_3). The increased concentration of In_2O_3 NPs caused a rise in the number of groups or

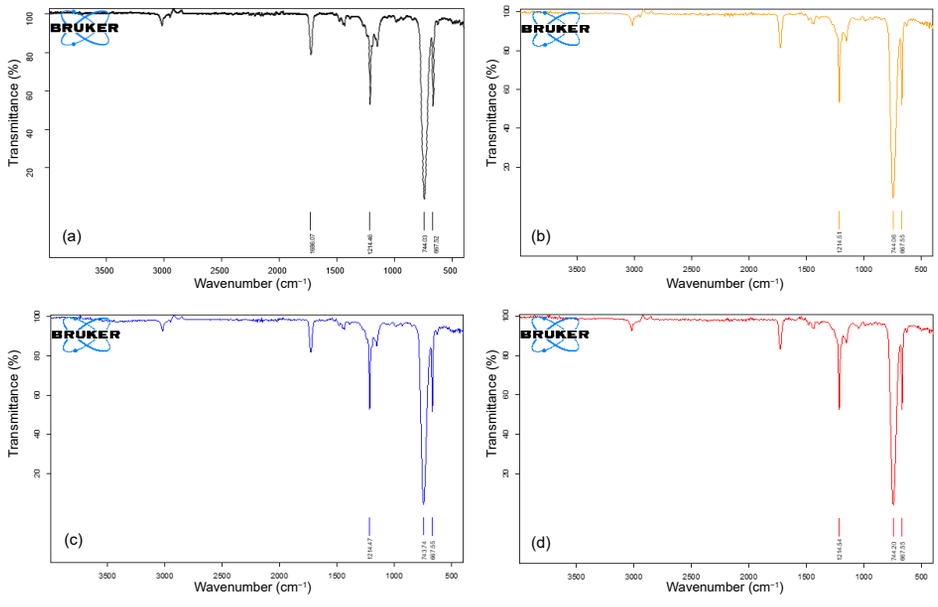

Fig. 11 FTIR spectrum for the pure PMMA and PMMA with varying content of In_2O_3 nanocomposite: **(a)** pure PMMA, **(b)** 1.2 wt.% In_2O_3 NPs, **(c)** 2.4 wt.% In_2O_3 NPs, and **(d)** 3.6wt.% In_2O_3 NPs.

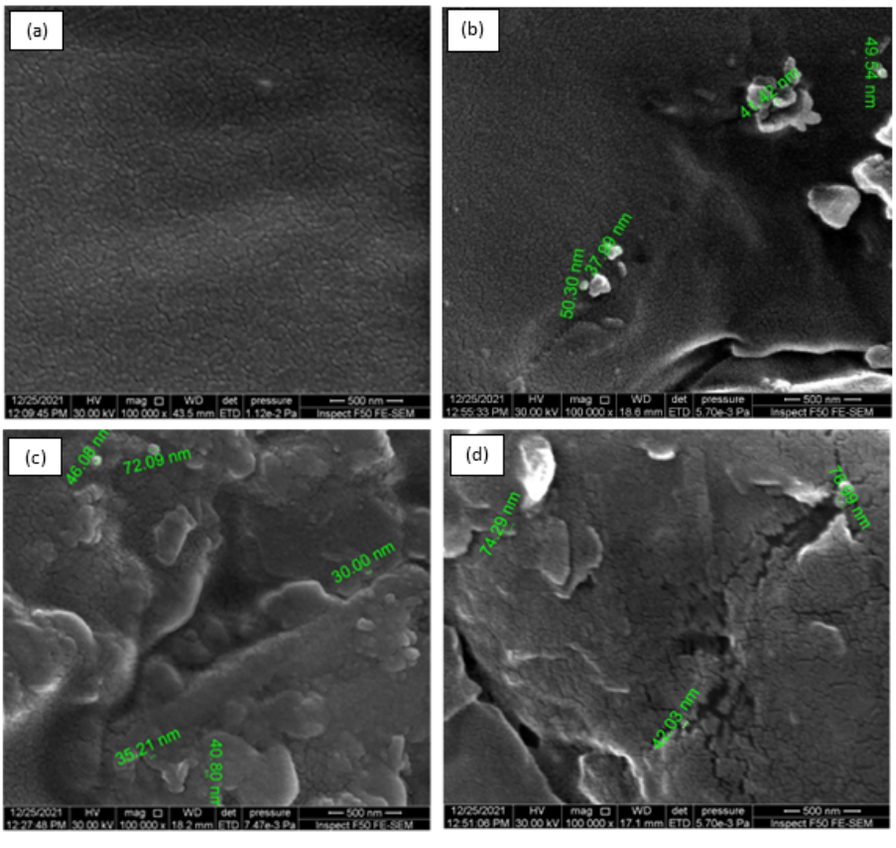

Fig. 12 FE-SEM images for pure PMMA and PMMA with variable content of In_2O_3 nanocomposite.

fragments that spread out on the top surface of the nanocomposites [39].

We then evaluated the antimicrobial activity of the PMMA/In_2O_3 nanocomposites against Gram-positive *S. aureus* and Gram-negative *E. coli* (Fig. 13). The nanocomposite films produced a larger zone of inhibited growth of *S. aureus* than that of *E. coli*. The inhibition zone increased in size with the increase in concentration of In_2O_3 NPs, reaching the largest size of 1.46 mm for inhibition of *S. aureus* growth with 3.6 wt.% In_2O_3 NPs (Table 3). The anti-microbial properties of nanostructures are attributed to the existence of reactive oxygen species (ROS) generated

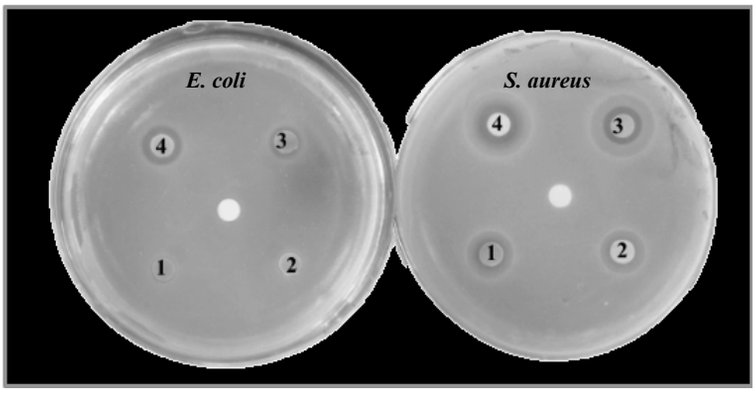

Fig. 13 Inhibition zones of PMMA/In_2O_3 nanocomposite films on culture plates of *S. aureus* and *E. coli:* 1-pure PMMA; 2-PMMA/1.2 wt.% In_2O_3 NPs; 3-PMMA/2.4 wt.% In_2O_3 NPs; 4-PMMA/3.6 wt.% In_2O_3 NPs.

by the NPs. Nanocomposite NPs are positively charged while bacteria have negative charges. Consequently, the bacteria will experience oxidation and death due to the electromagnetic contact. ROS, including radicals such as superoxide (O^{-2}), hydroxyl (OH), and hydrogen peroxide (H_2O_2) [40], mainly cause the antibacterial activities of nanocomposites containing NP, and singlet oxygen ($^1O_2$) most probably causes the degradation of bacterial proteins and DNA.

Table 3 Diameter of inhibition zone of PMMA/In_2O_3 nanocomposite films on growth of *S. aureus* and *E. coli*

Sample	Diameter of inhibition zone (mm)	
	E. coli	*S. aureus*
PMMA	0	0
PMMA/1.2 wt.% In_2O_3	0.85	0.97
PMMA/2.4 wt.% In_2O_3	1.15	1.29
PMMA/3.6 wt.% In_2O_3	1.31	1.46

Conclusion

This study successful used a casting method to prepare PMMA/In_2O_3 nanocomposites. FTIR analysis proved that the In_2O_3 NPs and the PMMA polymer matrix did not chemically interact. FE-SEM demonstrated that the In_2O_3 NPs were homogenously distributed throughout the polymer PMMA matrix. The optical characteristics were explained by the increase in the ratio of In_2O_3 NPs in the PMMA, producing an increase in the absorbance, absorption coefficient, refractive index, extinction coefficient, and real energy band gap, whereas a decrease in the transmittance and indirect energy gap occurred. Finally, the PMMA/In_2O_3 films demonstrated antibacterial activity against Gram-positive *S. aureus* and Gram-negative *E. coli* that exhibited a positive correlation with the concentration of In_2O_3 NPs (3.6 wt.%), with a maximum inhibition zone size of 1.46 mm for *S. aureus*.

CRediT Author Statement

Musaab Khudhur Mohammed: conceptualization, investigation, methodology, project administration, supervision, visualization, writing original draft, writing–review, and editing. **Noor Ali Sami:** data curation, formal analysis, and methodology. **Mohanad Abdul Salam:** investigation and writing original draft. **Reem Tuama Yousif:** software and resources. **Khansaa Haleem Mohsin:** writing–review and editing.

Conflict of Interests

The authors declared no conflict of interests regarding the content of this article.

References

[1] R. Moriche, M. Sánchez, A. Jiménez-Suárez, et al. Electrically conductive functionalized-GNP/epoxy based composites: From nanocomposite to multiscale glass fibre composite material. *Composites Part B*: *Engineering*, 2016, 98: 49−55. https://doi.org/10.1016/j.compositesb.2016.04.081

[2] S. Doagou-Rad, A. Islam, T.D. Merca. An application-oriented roadmap to select polymeric nanocomposites for advanced applications: A review. *Polymer Composites*, 2020, 41(4): 1153−1189. https://doi.org/10.1002/pc.25461

[3] C.A. Harper, E.M. Petrie. Plastics Materials and Processes: A Concise Encyclopedia. Wiley, 2003. https://doi.org/10.1002/0471459216

[4] S.S. Chiad, K.H. Abass, T.H. Mubarak, et al. Fabrication

and study the structure, optical and dispersion parameters. *Journal of Global Pharma Technology*, 2019, 11(4): 369−375.

[5] E.J. Tang, G.X. Cheng, X.L. Ma. Preparation of nano-ZnO/PMMA composite particles via grafting of the copolymer onto the surface of zinc oxide nanoparticles. *Powder Technology*, 2006, 161(3): 209−214. https://doi.org/10.1016/j.powtec.2005.10.007

[6] E. Marin, E. Mukai, M. Boschetto, et al. Antibacterial 3D-printed PMMA/ceramic composites. 2021, bioXiv: 2021.10.11.463892. https://doi.org/10.1101/2021.10.11.463892

[7] D. Ali Sabur, A. Hashim, A. Hadi, et al. Enhancement of optical properties in In_2O_3-doped PVA/PEG nanostructured films for optoelectronic applications. *Revue Des Composites et Des Matériaux Avancés*, 2023, 33(6): 411−417. https://doi.org/10.18280/rcma.330608

[8] N. Hayder, A. Hashim, M. Ali Habeeb, et al. Analysis of dielectric properties of PVA/PEG/In_2O_3 nanostructures for electronics devices. *Revue Des Composites et Des Matériaux Avancés*, 2022, 32(5): 261−264. https://doi.org/10.18280/rcma.320507

[9] R.E. Smith, V.M. Badner, D.E. Morse, et al. Maternal risk indicators for childhood caries in an inner city population. *Community Dentistry and Oral Epidemiology*, 2002, 30(3): 176−181. https://doi.org/10.1034/j.1600-0528.2002.300303.x

[10] M.M. Bagheri-Mohagheghi, N. Shahtahmasebi, E. Mozafari, et al. Effect of the synthesis route on the structural properties and shape of the indium oxide (In_2O_3) nano-particles. *Physica E*: *Low-Dimensional Systems and Nanostructures*, 2009, 41(10): 1757−1762. https://doi.org/10.1016/j.physe.2009.06.009

[11] Z.A. Husain, A.A. Majeed, R.T. Rasheed, et al. Antibacterial activity of In_2O_3 nanopowders prepared by hydrothermal method. *Materials Today*: *Proceedings*, 2021, 42: 1816−1821. https://doi.org/10.1016/j.matpr.2020.12.189

[12] G.D. Liu. Synthesis, characterization of In_2O_3 nanocrystals and their photoluminescence property. *International Journal of Electrochemical Science*, 2011, 6(6): 2162−2170. https://doi.org/10.1016/s1452-3981(23)18174-0

[13] A. Kolmakov, D.O. Klenov, Y. Lilach, et al. Enhanced gas sensing by individual SnO_2 nanowires and nanobelts functionalized with Pd catalyst particles. *Nano Letters*, 2005, 5(4): 667−673. https://doi.org/10.1021/nl050082v

[14] K.M. Varier, M. Gudeppu, A. Chinnasamy, et al. Nanoparticles: antimicrobial applications and its prospects. In: Environmental Chemistry for a Sustainable World. *Cham*: *Springer International Publishing*, 2019 321−355. https://doi.org/10.1007/978-3-030-04477-0_12

[15] H.H. Li, Q.S. Chen, J.W. Zhao, et al. Enhancing the antimicrobial activity of natural extraction using the synthetic ultrasmall metal nanoparticles. *Scientific Reports*, 2015, 5: 11033. https://doi.org/10.1038/srep11033

[16] I. Armentano, C.R. Arciola, E. Fortunati, et al. The interaction of bacteria with engineered nanostructured polymeric materials: A review. *The Scientific World Journal*, 2014, 2014: 410423. https://doi.org/10.1155/2014/410423

[17] A.A. Mohammed, M. Ali Habeeb. Modification and development of the structural, optical and antibacterial characteristics of PMMA/Si_3N_4/TaC nanostructures. *Silicon*, 2023, 15(12): 5163−5174. https://doi.org/10.1007/s12633-023-02426-2

[18] A.M. Kadim, K.H. Abass, K, Abdali, et al. Effect of loading corn starch nanoparticles on the morphological, optical, and dielectric behaviors of PVA/PMMA/PAAm polymer blend for optoelectronic and antibacterial applications. *Nano Biomedicine and Engineering*, 2024, 16(1): 119−127. https://doi.org/10.26599/NBE.2024.9290049

[19] P. Phukan, D. Saikia. Optical and structural investigation of CdSe quantum dots dispersed in PVA matrix and photovoltaic applications. *International Journal of Photoenergy*, 2013, 2013: 728280. https://doi.org/10.1155/2013/728280

[20] Q.M. Luo, Y.Y. Shan, X. Zuo, et al. Anisotropic tough poly(vinyl alcohol)/graphene oxide nanocomposite hydrogels for potential biomedical applications. *RSC Advances*, 2018, 8(24): 13284−13291. https://doi.org/10.1039/c8ra00340h

[21] M.K. Mohammed, G. Al-Dahash, A. Al-Nafiey. Fabrication and characterization of the PMMA/G/Ag nanocomposite by pulsed laser ablation (PLAL). *Nano Biomedicine and Engineering*, 2022, 14(1): 15−22. https://doi.org/10.5101/nbe.v14i1.p15-22

[22] A.A. Khadayeir, K.H. Abass, S.S. Chiad, et al. Study the influence of antimony trioxide (Sb_2O_3) on optical properties of (PVA-PVP) composites. *Journal of Engineering and Applied Sciences*, 2018, 13(22): 9689−9692.

[23] H.T. Salloom, A.S. Jasim, T.K. Hamad. Synthesis and optical characterization of Ag/PVA nanocomposites films. *Journal of Al-Nahrain University Science*, 2017, 20(4): 56−63. https://doi.org/10.22401/jnus.20.4.10

[24] S.S. Mousavi, B. Sajad, M.H. Majlesara. Fast response ZnO/PVA nanocomposite-based photodiodes modified by graphene quantum dots. *Materials & Design*, 2019, 162: 249−255. https://doi.org/10.1016/j.matdes.2018.11.037

[25] H.M. Zidan, E.M. Abdelrazek, A.M. Abdelghany, et al. Characterization and some physical studies of PVA/PVP filled with MWCNTs. *Journal of Materials Research and Technology*, 2019, 8(1): 904−913. https://doi.org/10.1016/j.jmrt.2018.04.023

[26] H.M. Zidan, M. Abu-Elnader. Structural and optical properties of pure PMMA and metal chloride-doped PMMA films. *Physica B*: *Condensed Matter*, 2005, 355(1-4): 308−317. https://doi.org/10.1016/j.physb.2004.11.023

[27] A. Rahma, M.M. Munir, Khairurrijal, et al. Intermolecular interactions and the release pattern of electrospun curcumin-polyvinyl(pyrrolidone) fiber. *Biological and Pharmaceutical Bulletin*, 2016, 39(2): 163−173. https://doi.org/10.1248/bpb.b15-00391

[28] L.K. Mireles, M.R. Wu, N. Saadeh, et al. Physicochemical characterization of polyvinyl pyrrolidone: A tale of two polyvinyl pyrrolidones. *ACS Omega*, 2020, 5(47): 30461−30467. https://doi.org/10.1021/acsomega.0c04010

[29] T.S. Soliman, S.A. Vshivkov, S.I. Elkalashy. Structural, thermal, and linear optical properties of SiO_2 nanoparticles dispersed in polyvinyl alcohol nanocomposite films. *Polymer Composites*, 2020, 41(8): 3340−3350. https://doi.org/10.1002/pc.25623

[30] J. Fal, K. Bulanda, J. Traciak, et al. Electrical and optical properties of silicon oxide lignin polylactide (SiO_2-L-PLA). *Molecules*, 2020, 25(6): 1354. https://doi.org/10.3390/molecules25061354

[31] M.A. Habeeb. Enhancement of structural and mechanical properties for (PVA-PAAm) by adding titanium nanoparticles. *Australian Journal of Basic and Applied Sciences*, 2014, 8(17): 1−9.

[32] A. Paydayesh, A.A. Azar, A.J. Arani. Investigation the effect of graphene on the morphology, mechanical and thermal properties of PLA/PMMA blends. *Ciência e Natura*, 2015, 37: 15.

[33] S.S. Nemah, Z.A. Hasan. Influence of silver nanoparticles

on optical properties for (PS-PMMA) blend. *Journal of Global Pharma Technology*, 2019, 11(7): 325−330.

[34] M.R. Mas Haris, S. Kathiresan, S. Mohan. FT-IR and FT-Raman spectra and normal coordinate analysis of poly methyl methacrylate. *Der Pharma Chemica*, 2010, 2(4): 316−323.

[35] M.O. Bensaid, L. Ghalouci, S. Hiadsi, et al. Molecular mechanics investigation of some acrylic polymers using SPASIBA force field. *Vibrational Spectroscopy*, 2014, 74: 20−32. https://doi.org/10.1016/j.vibspec.2014.07.001

[36] S. Ramesh, K.H. Leen, K. Kumutha, et al. FTIR studies of PVC/PMMA blend based polymer electrolytes. *Spectrochimica Acta Part A*: *Molecular and Biomolecular Spectroscopy*, 2007, 66(4-5): 1237−1242. https://doi.org/10.1016/j.saa.2006.06.012

[37] V.N. Rai, C. Mukherjee, B. Jain. Optical properties (uv-vis and ftir) of gamma irradiated polymethyl methacrylate (pmma). 2016, arXiv: 1611.02129. http://arxiv.org/abs/1611.02129

[38] A.P. Indolia, M.S. Gaur. Optical properties of solution grown PVDF-ZnO nanocomposite thin films. *Journal of Polymer Research*, 2012, 20(1): 43. https://doi.org/10.1007/s10965-012-0043-y

[39] Y.T. Prabhu, K.V. Rao, B.S. Kumari, et al. Synthesis of Fe_3O_4 nanoparticles and its antibacterial application. *International Nano Letters*, 2015, 5(2): 85−92. https://doi.org/10.1007/s40089-015-0141-z

[40] S.S. Behera, J.K. Patra, K. Pramanik, et al. Characterization and evaluation of antibacterial activities of chemically synthesized iron oxide nanoparticles. *World Journal of Nano Science and Engineering*, 2012, 2(4): 196−200. https://doi.org/10.4236/wjnse.2012.24026